Food Chemistry 407 (2023) 135156

Contents lists available at ScienceDirect

Food Chemistry

journal homepage: www.elsevier.com/locate/foodchem

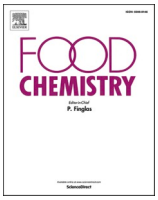

# Reactivity of Fe(III)-containing pyrophosphate salts with phenolics: complexation, oxidation, and surface interaction

Judith Bijlsma [a,‡], Neshat Moslehi [b,‡], Krassimir P. Velikov [c,d,e], Willem K. Kegel [b], Jean-Paul Vincken [a], Wouter J.C. de Bruijn [a,*]

[a] Laboratory of Food Chemistry, Wageningen University & Research, Bornse Weilanden 9, P.O. Box 17, 6700 AA, Wageningen, the Netherlands
[b] Van 't Hoff Laboratory for Physical and Colloidal Chemistry, Debye Institute for Nanomaterials Science, Utrecht University, Padualaan 8, 3584 CH Utrecht, the Netherlands
[c] Unilever Innovation Centre Wageningen, Bronland 14, 6708 WH Wageningen, the Netherlands
[d] Soft Condensed Matter, Debye Institute for Nanomaterials Science, Utrecht University, Princetonplein 5, 3584 CC Utrecht, the Netherlands
[e] Institute of Physics, University of Amsterdam, Science Park 904, 1098 XH Amsterdam, the Netherlands

ARTICLE INFO

*Keywords:*
Mixed calcium-iron (III) pyrophosphate salts
Food fortification
Iron supplementation
Polyphenols
Flavonoids

ABSTRACT

Mixed pyrophosphate salts with the general formula $Ca_{2(1-x)}Fe_{4x}(P_2O_7)_{(1+2x)}$ potentially possess less iron-phenolic reactivity compared to ferric pyrophosphate (FePP), due to decreased soluble Fe in the food-relevant pH range 3–7. We investigated reactivity (i.e., complexation, oxidation, and surface interaction) of FePP and mixed salts (with x = 0.14, 0.15, 0.18, and 0.35) in presence of structurally diverse phenolics. At pH 5–7, increased soluble iron from all salts was observed in presence of water-soluble phenolics. XPS confirmed that water-soluble phenolics solubilize iron after coordination at the salt surface, resulting in increased discoloration. However, color changes for mixed salts with $x \leq 0.18$ remained acceptable for slightly water-soluble and insoluble phenolics. Furthermore, phenolic oxidation in presence of mixed salts was significantly reduced compared to FePP at pH 6. In conclusion, these mixed Ca-Fe(III) pyrophosphate salts with $x \leq 0.18$ can potentially be used in designing iron-fortified foods containing slightly water-soluble and/or insoluble phenolics.

## 1. Introduction

Fortification of food with iron is an effective approach to overcome the global iron deficiency (Allen, De Benoist, Dary, & Hurrell 2006). However, the addition of iron to foods is problematic due to its high reactivity with phenolic compounds present in the food. Complexation and oxidation of phenolics in the presence of iron ions cause an undesirable change in the organoleptic properties of the food products such as changes in taste and texture, or discoloration resulting from dark brown or black color formation upon iron-phenolic complexation (Bijlsma, de Bruijn, Velikov, & Vincken, 2022; Habeych, van Kogelenberg, Sagalowicz, Michel, & Galaffu, 2016; Janssen et al., 2019). Moreover, the reactivity of iron with phenolic compounds can hinder iron bioavailability and can consequently reduce iron uptake in the human body (Andre et al., 2015). One strategy to counter the reactivity problem is to use a poorly water-soluble iron-containing salt such as iron (III) pyrophosphate (FePP) (Habeych et al., 2016; Hurrell, 2002). However, even addition of iron as FePP cannot fully prevent discoloration in phenolic-rich foods (Dueik, Chen, & Diosady, 2017; Hurrell et al., 2004). Moreover, the poor solubility of FePP in the gastrointestinal tract results in limited iron bioavailability (Dueik et al., 2017; Hurrell et al., 2004). Our previous study indicated that including calcium as a divalent metal, alongside iron, in the pyrophosphate salt matrix can be utilized to design potential dual-fortificants. The soluble iron concentration from these mixed salts, with the general formula of $Ca_{2(1-x)}Fe_{4x}P_2O_{7(1+2x)}$, was reduced by up to eightfold at food-relevant pH ranges, whereas it was enhanced up to fourfold in gastric relevant pH ranges, compared to FePP (Moslehi, Bijlsma, De Bruijn, Velikov, Vincken, & Kegel, 2022). Additionally, the inclusion of calcium as the second metal in the mixed Ca-Fe(III) pyrophosphate salt is expected to lower the iron content at the surface of these salts and therefore lead to a decrease in reactivity, with respect to FePP. Despite much lower soluble

* Corresponding author.
*E-mail addresses:* judith.bijlsma@wur.nl (J. Bijlsma), n.moslehi@uu.nl (N. Moslehi), krassimir.velikov@unilever.com (K.P. Velikov), w.k.kegel@uu.nl (W.K. Kegel), jean-paul.vincken@wur.nl (J.-P. Vincken), wouter.debruijn@wur.nl (W.J.C. de Bruijn).
‡ Judith Bijlsma and Neshat Moslehi contributed equally to this work.

https://doi.org/10.1016/j.foodchem.2022.135156
Received 15 July 2022; Received in revised form 16 November 2022; Accepted 3 December 2022
Available online 6 December 2022

iron concentration and the expected lower iron content at the surface, the mixed Ca-Fe(III) pyrophosphate salts previously did not show noticeably less reactivity compared to FePP in a black tea system (Moslehi et al., 2022). To create a clear link between the dissolution behavior of iron from these mixed salts and the observed reactivity of the salts, the current work aims to investigate the soluble iron from the Ca-Fe(III) pyrophosphate salts in the presence of phenolics as representative food matrix compounds that can react with iron.

We previously observed that the solubility of flavonoids affects the soluble iron concentration (Bijlsma et al., 2022). Therefore, a set of six model phenolic compounds with different chemical properties, most notably different water solubilities, were selected (Fig. 1) to investigate their interaction behavior with the mixed Ca-Fe(III) pyrophosphate salts. The chosen phenolic compounds also differ in the most likely Fe (III)-complexation sites, as is highlighted in Fig. 1 (Bijlsma et al., 2022; Mohammed, Rashid-Doubell, Cassidy, & Henari, 2017; Nkhili, Loonis, Mihai, El Hajji, & Dangles, 2014; Perron & Brumaghim, 2009). The solubility values are calculated and shown as *logS* (i.e., the logarithm of water-solubility in molar) in Fig. 1. Catechol, caffeic acid, and epicatechin show *logS* values ranging from 0 to − 2, which was previously classified as water-soluble by Sorkun and co-authors (Sorkun, Khetan, & Er, 2019). Accordingly, quercetin and apigenin ($-4 < logS < -2$) are slightly soluble, and curcumin ($logS < -4$) is insoluble. These phenolics were chosen because they are common in food products (Delgado, Issaoui, & Chammem, 2019; Habeych et al., 2016), except for catechol which was selected as a model for *o*-dihydroxybenzenes.

Deprotonation of the hydroxyl substituents is a prerequisite for iron coordination (Perron & Brumaghim, 2009). The $pK_a$ values of the hydroxyl groups are indicated in Fig. 1. It should be noted that in the presence of iron ions the deprotonated state of the phenolics is stabilized and that the apparent $pK_a$ values will therefore be lowered to values in the range of pH 5–8 for the phenol moiety (Hider, Liu, & Khodr, 2001). The actual $pK_a$ lowering effect is dependent on the structural features of the phenolic compound and the stabilization of the resulting anion (Silva, Kong, & Hider, 2009). The stoichiometry and color of iron-phenolic complexes (e.g. 1:1, 1:2, 2:1, etc) and the preferred iron-binding sites are dependent on the solvent, the pH of the sample, iron salt, and the phenolic structure (Bijlsma, de Bruijn, Hageman, Goos, Velikov, & Vincken, 2020; Kasprzak, Erxleben, & Ochocki, 2015). For caffeic acid, coordination of metals to the catecholate moiety is suggested to be preferred over coordination to the carboxylate moiety, because of the higher electron density of the catecholate oxygens and the stable five-membered ring that is formed upon coordination.

We hypothesize that mixed Ca-Fe(III) pyrophosphate salts will show decreased reactivity towards phenolic compounds at food-relevant pH values compared to FePP due to (i) decreased soluble iron concentration from the salts at pH 3–7, and (ii) decreased iron content at the surface of these salts. To this end, we evaluate iron dissolution behavior, spectral changes indicating iron-mediated complexation, oxidation of the phenolic compounds, and reactions at the surface of these salts.

## 2. Materials and methods

### 2.1. Chemicals

Hydrochloric acid (37 wt%), sodium hydroxide (≥98 wt%), nitric acid (65 wt%), iron(II) sulfate heptahydrate (≥99 wt%), 3-(2-pyridyl)-5,6-diphenyl-1,2,4-triazine-*p,p′*-disulfonic acid monosodium salt hydrate (≥97 wt%; ferrozine), ferric chloride hexahydrate ($FeCl_3{\cdot}6H_2O$, ≥ 99 wt%), tetrasodium pyrophosphate decahydrate ($Na_4P_2O_7{\cdot}10H_2O$, ≥ 99 wt%, NaPP), calcium dichloride ($CaCl_2$, ≥ 93 wt%), quercetin hydrate (≥95 wt%), 1,2-dihydroxybenzene (≥99 wt%; catechol), caffeic acid (≥98 wt%), and curcumin (≥94 wt%), were obtained from Merck Life Science (Darmstadt, Germany). (−)-Epicatechin (≥97 wt%) was purchased from TCI Europe NV (Zwijndrecht, Belgium), apigenin (≥98 wt%) from Indofine Chemical Company (Hillsborough, NJ, USA), and ascorbic acid (≥99 wt%) was obtained from VWR International (Radnor, PA, USA). ULC-MS grade acetonitrile (ACN) and water, both containing 0.1 vol% formic acid (FA) were purchased from Biosolve (Valkenswaard, The Netherlands). Water for other purposes than UHPLC was prepared using a Milli-Q (MQ) water purification system (Merck Millipore, Billerica, MA, USA).

### 2.2. Preparation of the CaPP, FePP, and mixed Ca-Fe(III) pyrophosphate salts

Iron (III) pyrophosphate ($Fe_4(P_2O_7)_3$, FePP), calcium pyrophosphate ($Ca_2P_2O_7$, CaPP), and mixed Ca-Fe(III) pyrophosphate salts with different iron to calcium ratios according to the general formula $Ca_{2(1-x)}Fe_{4x}(P_2O_7)_{(1+2x)}$ with x = 0.14, 0.15, 0.18, and 0.35 were prepared using a coprecipitation method as described elsewhere (Moslehi et al., 2022). Uniformity in morphology was confirmed by transmission electron microscopy (TEM). Bulk morphology and chemical compositions of the mixed salts, obtained by energy-dispersive spectroscopy (TEM-EDX) are reported in the **supplementary information**, **Fig. S1**.

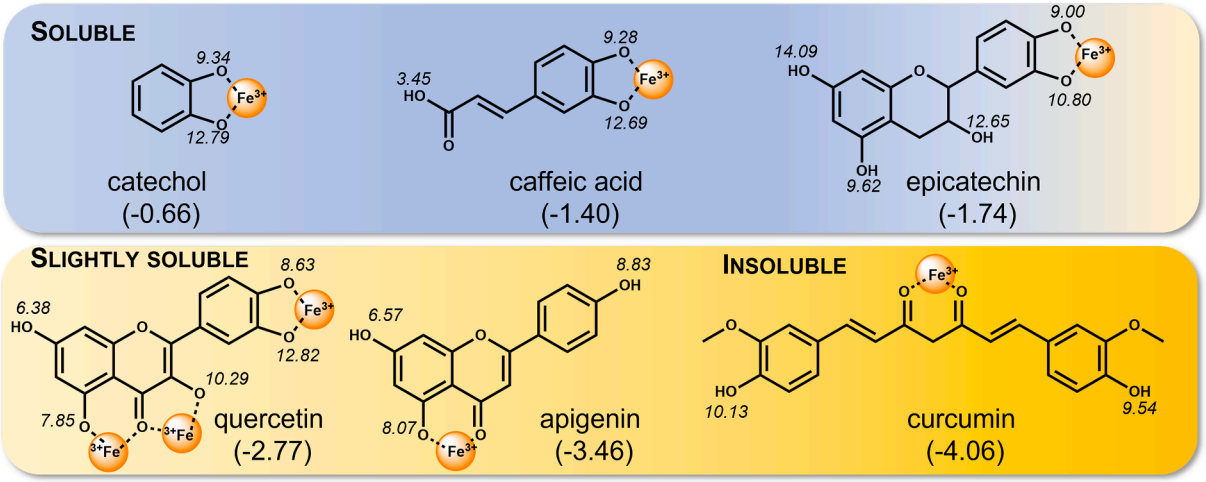


**Fig. 1.** Structure of phenolic compounds used in this study, and the most likely Fe(III)-complexation sites. The pKa values for hydroxyl groups of the phenolics are shown in italic, and *logS* values of the phenolic compounds are given in brackets. *LogS* values were calculated using MarvinSketch 22.3 (ChemAxon). Based on the *logS* values, the water-solubility of the phenolics was classified as soluble, slightly soluble, and insoluble.

### 2.3. Reactivity of the CaPP, FePP, and mixed Ca-Fe(III) pyrophosphate salts with phenolics

The CaPP, FePP, and the mixed Ca-Fe(III) pyrophosphate salts were redispersed in water by stirring (~250 rpm) with a magnetic stir bar (final amount of salt 10 mg/ml) followed by the addition of aqueous solutions (i.e., catechol, caffeic acid, and epicatechin) or dispersions (i.e., quercetin, apigenin, and curcumin) of the phenolics to reach a final concentration of 5 mM phenolic. Next, the pH of the dispersions was adjusted using a pH-stat device (Metrohm, Herisau, Switzerland) by automatic titration using 0.1 M HCl or 0.1 M NaOH. Subsequently, the dispersions with pH values ranging from one to eleven (steps of one) were incubated for 2 h at 23 °C under continuous stirring at 1000 rpm. After incubation, the pH of each sample was measured again to determine the final pH. Finally, the samples were centrifuged at 15,000 × *g* for 10 min, and the supernatants were separated to quantify the dissolved iron concentration and obtain the absorbance spectra.

#### 2.3.1. Iron concentration measurement by ferrozine-based colorimetric assay

The total iron in the solution was quantified using a ferrozine-based colorimetric assay (Stookey, 1970) with slight adaptations as described elsewhere (Moslehi et al., 2022). In short, the absorbance of the iron(II)-ferrozine complex at 565 nm was measured at room temperature in a SpectraMax M2e (Molecular Devices, Sunnyvale, CA, USA). All measurements were performed in duplicate and quantification of the total dissolved iron was performed with a calibration curve of $FeSO_4$ (0.0078 – 1 mM, $R^2 > 0.99$). The relative change in soluble iron concentration after addition of phenolics was defined according to equation (1).

$$\text{Relative change} = \frac{\text{iron solubility with phenolics} - \text{iron solubility blank}}{\text{iron solubility blank}} \quad (1)$$

The iron quantification in presence of phenolics by the ferrozine assay was verified independently using inductively coupled plasma–atomic emission spectroscopy (ICP-AES) (**supplementary information**, **Method S1)**.

### 2.4. Monitoring reactivity and discoloration by UV–vis spectroscopy

The reactivity of the pure FePP and CaPP, as well as the mixed Ca-Fe (III) pyrophosphate salts in the presence of the different phenolic compounds, was monitored using ultraviolet–visible light (UV–vis) spectroscopy. After centrifugation, 200 µl sample was transferred to a Corning® UV-transparent flat-bottom polystyrene 96-well plate (Sigma Aldrich, St. Louis, MO, USA). Spectra were recorded in the range from 250 to 750 nm in a SpectraMax M2e (Molecular Devices, Sunnyvale, CA, USA), at room temperature. The color of the samples was visualized by taking an image (OnePlus 7 T, Beijing, China) of the Eppendorf tubes with a uniform light source against a white background. The images were evaluated using the $L^*a^*b^*$ color space (i.e., $L^*$ dark or light, $a^*$ red vs green, $b^*$ yellow vs blue). The values were extracted using the standard image analysis software (Photoshop CC 2021, Adobe). In this procedure, the $L^*a^*b^*$ value was taken at five different spots in the supernatant and five spots in the precipitate (**supplementary information**, **Fig. S2**). The degree of difference between the phenolic blank and the samples of phenolics in presence of the iron-containing salts, $\Delta Eab$, corresponds to the distance between two points within the $L^*a^*b^*$ color space. The $\Delta Eab$ value (e.g., the absolute value of the color difference, not the direction) was calculated according to equation (2) (Araki et al., 2017; Poynton, 2012).

$$\Delta Eab = \left[\left(L_0^* - L_x^*\right)^2 + \left(a_0^* - a_x^*\right)^2 + \left(b_0^* - b_x^*\right)^2\right]^{1/2} \quad (2)$$

where $L_0^*$, $a_0^*$, $b_0^*$ and $L_x^*$, $a_x^*$, $b_x^*$ are the color space values for the blank phenolic and the phenolic exposed to the iron-containing salts, respectively.

### 2.5. Monitoring phenolics solubility and oxidation by RP-UHPLC-PDA-ESI-IT-$MS^n$

The water-solubility of the blank phenolics at pH 3, 6, and 8, and oxidation of epicatechin and quercetin at pH 3, 6, and 8 after incubation with the iron-containing salts, were analyzed by reversed-phase ultra-high performance liquid chromatography coupled to electrospray ionization ion trap mass spectrometry (RP-UHPLC-PDA-ESI-IT-$MS^n$). Here, pH 3, 6, and 8 were chosen as they respectively represent gastric, food, and intestinal conditions (Habeych et al., 2016; Tian, Blanco, Smoukov, Velev, & Velikov, 2016).

To test the oxidation of epicatechin and quercetin after incubation with the iron-containing salts, the supernatants from section 2.3 were separated from the precipitate to obtain the water-soluble fractions. The precipitates were then solubilized in DMSO (100 vol%), which is known to be a suitable solvent for metal:ligand systems (Bijlsma et al., 2022; El-Sherif, Shoukry, & Abd-Elgawad, 2013). The resulting suspensions were centrifuged once more (at 15,000×*g* for 5 min) and the supernatants were separated to obtain the DMSO-soluble fractions. Phenolics' recovery and their oxidation products in the water-soluble and DMSO-soluble fractions were separated on a Thermo Vanquish UHPLC system (Thermo Scientific, San Jose, CA, USA) equipped with an autosampler, a pump, and a photodiode array (PDA) detector. A sample (1 µl) was injected on an Acquity UPLC BEH C18 column (150 mm × 2.1 mm i.d., 1.7 µm) with a VanGuard (5 mm × 2.1 mm i.d., 1.7 µm) guard column of the same material (Waters, Milford, MA). Water (A) and acetonitrile (B), both acidified with 0.1 vol% formic acid, were used as eluents. The flow rate was 400 µl $min^{-1}$, and the temperature of the column oven was 45 °C with the post-column cooler set to 40 °C. The elution profiles can be found in the **supplementary information** (**Method S2**). The PDA detector was set to measure the wavelength range of 190 – 680 nm. Mass spectrometric data were acquired using a Velos Pro ion trap mass spectrometer (Thermo Scientific) equipped with a heated electrospray ionization probe (ESI-IT-$MS^n$) coupled in-line to the Vanquish UHPLC system. Nitrogen was used as a sheath gas (50 arbitrary units) and auxiliary gas (13 arbitrary units). Data were collected over the *m/z* range of 100 – 1,500 in negative and positive ionization mode by using source voltages of 2.5 and 3.5 kV, respectively. For both modes, the S-lens RF level was set at 67%, the ion transfer tube and the source heater temperatures were 263 and 425 °C, respectively. Data-dependent $MS^2$ analysis was performed on the most intense ion by collision-induced dissociation (CID) with a normalized collision energy of 35%. A dynamic mass exclusion approach was used, in which the most intense ion was fragmented 3 times and was subsequently excluded from fragmentation for the following 5 s, allowing data-dependent $MS^2$ of less intense co-eluting compounds. Data acquisition and processing were performed using Xcalibur (version 4.1, Thermo Scientific). Quantification of phenolic was performed based on PDA peak area (280 nm) and an external calibration curve of the corresponding authentic standard (0.003 – 0.5 mM, in duplicate, $R^2 = 1.00$). To assess whether the change in phenolic recovery was statistically significant, ANOVA analysis was performed using IBM SPSS Statistic v23 software (SPSS Inc., Chicago, IL, USA). Tukey's *post hoc* comparisons (significant at $p < 0.05$) were carried out to evaluate the total concentration of the phenolics at different pH values in presence of the different salts.

### 2.6. Surface composition of the CaPP, FePP, and mixed Ca-Fe(III) pyrophosphate salts by X-ray photoelectron spectroscopy

The surface composition of CaPP, FePP, and Ca-Fe(III) pyrophosphate particles was determined by X-ray photoelectron spectroscopy (XPS), the sampling depth of XPS is 3–10 nm (Giesbers, Marcelis, & Zuilhof, 2013). The salts were also analyzed after incubation with epicatechin (pH 6) using the same incubation setup as in section 2.3. After

incubation, the samples were centrifuged at 5,000×*g* for 10 min and the precipitate was washed twice with water. Complete removal of water from the samples was ensured by overnight drying in a vacuum oven at 50 °C. Samples were prepared on indium foil. XPS measurements were performed using a JPS-9200 photoelectron spectrometer (JEOL ltd., Japan). All samples were analyzed using a focused monochromated Al Kα X-ray source (spot size of 300 μm), wide scans were recorded at a constant dwelling time of 50 ms and pass energies of 50 eV. The power of the X-ray source was 240 W (20 mA and 12 kV). The charge compensation was used during the XPS scans with an accelerating voltage of 2.8 eV and a filament current of 4.8 A. XPS wide-scan were obtained under ultrahigh-vacuum conditions (base pressure, $3 \times 10^{-7}$ Pa). The spectra were fitted with symmetrical Gaussian/Lorentzian (GL(30)) line shapes using CasaXPS (version 2.3.22PR1.0). All spectra were referenced to the C 1 s peak attributed to C–C and C–H bonds at 285.0 eV.

## 3. Results and discussion

### 3.1. Dissolution behavior of iron from FePP and the mixed Ca-Fe(III) pyrophosphate salts in the presence of phenolics

The dissolution of total iron from FePP and the mixed Ca-Fe(III) pyrophosphate salts in the presence of phenolic compounds was studied as a function of pH, using the ferrozine assay (Stookey, 1970). This assay was verified for the combination of epicatechin and all salts by comparison with the ICP-AES method (**supplementary information**, **Fig. S3**). The soluble iron concentration from 10 mg/ml dispersions of FePP and the four mixed salts in the presence of the six different phenolics was evaluated in water in the food-relevant pH range 3–7 (Fig. 2**A**). The dispersions were prepared based on an equal amount of the salts (10 mg/ml), no direct relationship was observed between the theoretical maximum iron concentration of the dispersion and the measured iron concentration in solution (**Table S1** of **supplementary information**). The soluble iron concentrations presented here were determined after two hours incubation of the salt dispersions, and are therefore not necessarily equal to the solubilities (i.e., the equilibrium saturation concentrations). We assume that the iron dissolution from the mixed salt was complete at that time point (Moslehi et al., 2022).

We confirmed experimentally that at pH 3, 6, and 8 epicatechin, caffeic acid, and catechol showed good water-solubility and that quercetin, apigenin, and curcumin were slightly soluble or insoluble in water in the absence of iron (**supplementary information**, **Fig. S4**).

At food-relevant pH values (3–7), the mixed salts with $x \leq 0.18$ exhibit a lower soluble iron concentration than FePP (Fig. 2**A**, blank). Additionally, the soluble iron concentration from the mixed salts with $x \leq 0.18$ depended on the pH and water-solubility of the phenolic compound as well.

In the range from pH 3 to 5, iron from the mixed Ca-Fe(III) pyrophosphate salts with $x \leq 0.18$ was (practically) insoluble regardless of the presence of phenolics, i.e., iron concentration in solution was <0.18 mM which equals < 0.1 g/l (Liangou, Florou, Psichoudaki, Kostenidou, Tsiligiannis, & Pandis, 2022). The theoretical maximum concentrations of dissolved iron from the salts, based on the initial amount of 10 mg/ml salt, are listed in **Table S1** of **supplementary information**. In the pH range from 3 to 5, the phenolics did not affect the iron dissolution because all hydroxyl groups are protonated (the apparent $pK_a$ range of phenolate is 5–8) and therefore do not coordinate iron (Hider et al., 2001). Upon increasing the pH from 5 to 7 the hydroxyl groups of the phenolics are deprotonated, leading to differential iron dissolution from the pyrophosphate salts for the different categories of phenolics

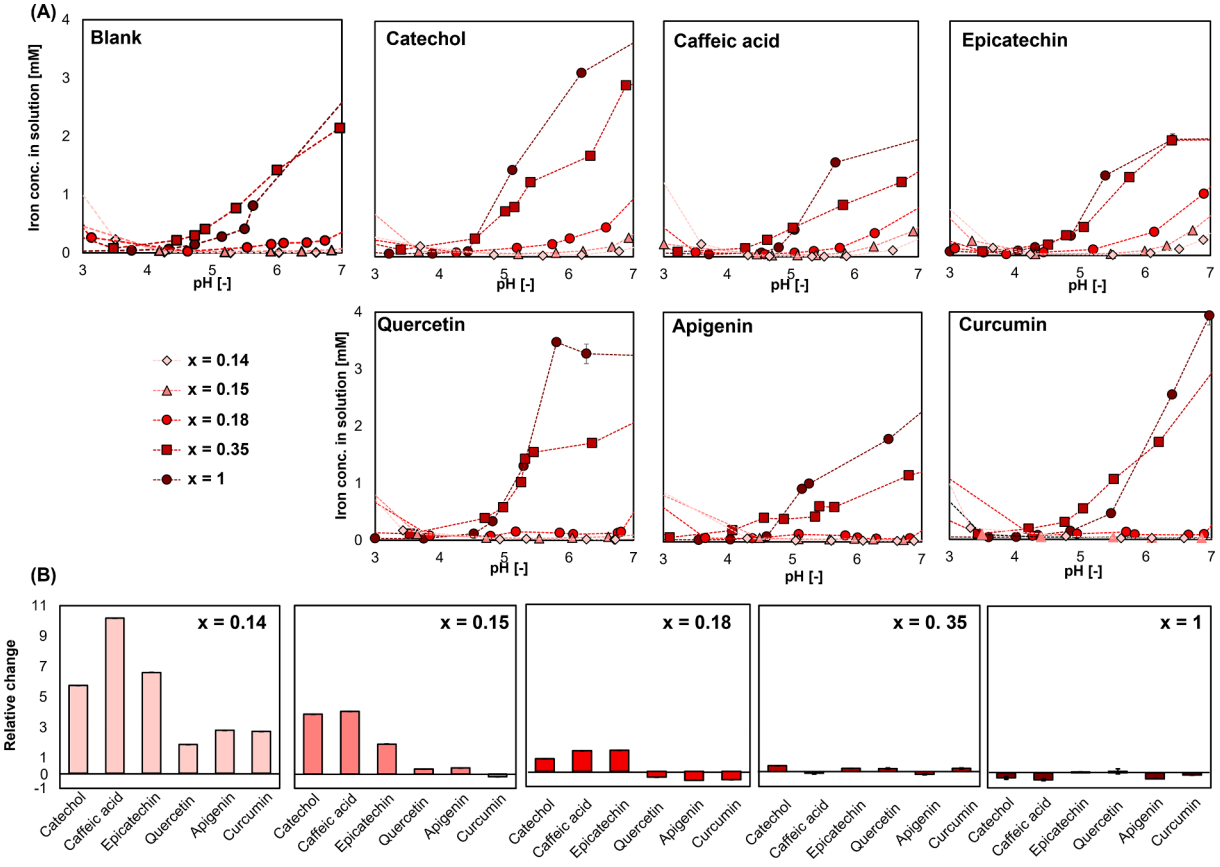


**Fig. 2.** (A) Dissolution behavior of iron at pH 3–7 from FePP (x = 1) and mixed Ca-Fe(III) pyrophosphate salts with x = 0.14, x = 0.15, x = 0.18, and x = 0.35, in the absence of phenolics (blank), and in presence of catechol, caffeic acid, epicatechin, quercetin, apigenin, and curcumin at 23 °C. (B) Relative change (equation (1), section 2.3.1) in the soluble iron concentration from the salts in presence of the phenolic compound compared to the absence of phenolic compound at pH 6–6.5.

(Fig. 2**A**). For the water-soluble phenolics (i.e., catechol, caffeic acid, and epicatechin), an up to 11-fold increase in soluble iron concentration from the mixed Ca-Fe(III) pyrophosphate salts with $x \leq 0.18$ was observed at pH 6–6.5 compared to the iron salt in the absence of the phenolics (Fig. 2**B**). However, in the presence of the slightly water-soluble (i.e., quercetin and apigenin) and insoluble phenolics (i.e., curcumin), the relative change in soluble iron concentration was lower compared to water-soluble phenolics and the iron remained practically insoluble. Interestingly, a higher dissolved iron concentration was measured for the salts with $x = 0.35$ and $x = 1$ in the presence of quercetin, compared to apigenin, despite the similar $pK_a$ and *logS* values for these flavonoids (Fig. 1**A**). We suggest that the observed difference in the measured iron concentration in solution is because a charged, and therefore soluble, iron-phenolic complex is more likely for quercetin than for apigenin. This is expected to be due to the multiple iron-binding sites in the case of quercetin (Malacaria, Corrente, Beneduci, Furia, Marino, & Mazzone, 2021) and the relatively high reported stability constant of iron-quercetin complexes resulting from the presence of a catecholate moiety (**Table S2**, **supplementary information**).

Furthermore, the salt with $x = 0.35$ showed the highest absolute soluble iron concentration among the mixed salts and was similar to FePP ($x = 1$) in the presence of all phenolics over the food-relevant pH range (3–7) (Fig. 2**A**). At pH 6–6.5 the soluble iron concentration from the salts with $x = 0.35$ and $x = 1$ was not affected by the solubility of the phenolic (Fig. 2**B**).

At pH < 3, in the blank and in presence of all phenolics, an increase in soluble iron concentration was observed from all mixed Ca-Fe(III) pyrophosphate salts compared to pure FePP (**supplementary information**, **Fig. S5**). No clear trend was observed below pH 3 between the category of the phenolic and the soluble iron. At pH > 7, which includes the intestinal pH range, irrespective of the phenolic compound, lower iron concentrations in solution were measured for all the mixed Ca-Fe (III) pyrophosphate salts compared to FePP. There was only one exception to this observation: For the salt with $x = 0.35$, at pH > 8 in the presence of epicatechin and caffeic acid, the soluble iron concentration was measured to be equal to and higher than that of FePP, respectively (**supplementary information Fig. S5**). Finally, the soluble iron from the mixed salts with $x = 0.14$ and 0.15 remained low (i.e., < 0.15 mM) and in line with the blank (no phenolics) in the presence of apigenin and curcumin at pH > 8.

The effect of temperature on the dissolution behavior of iron from the pyrophosphate salts in the presence of epicatechin was also investigated. The soluble iron concentration from the salts with $x \leq 0.18$ was observed to be similar at 23, 37, and 90 °C in the gastric and food-relevant pH ranges (**supplementary information**, **Fig. S6**). These results suggest that the soluble iron does not change in gastric conditions (37 °C), and after cooking (90 °C) (Swain, Newman, & Hunt, 2003).

### 3.2. Discoloration of CaPP, FePP, and mixed Ca-Fe(III) pyrophosphate salts with phenolics

The total absorbance and discoloration of the CaPP, FePP, and the mixed Ca-Fe(III) pyrophosphate salts in the presence of all phenolics was assessed at pH 6–6.5 (Fig. 3**A**). This pH range was explored as it is in the range of most food products, and more particularly savory concentrates, which is one of the preferred foods for iron-fortification (Moretti, Hurrell, & Cercamondi, 2018). The pH of three commercial savory concentrates was measured to be 6.27 ± 0.59. The color of the supernatants and the precipitates were evaluated visually (Fig. 3**B**) and according to the *CIELab** color space. The *L*a*b** values were used to calculate the Δ*Eab* as a qualitative tool for the color difference between the supernatant and precipitate after exposing the phenolics to the iron-containing salts (Fig. 3**C**). It was assumed that when the Δ*Eab* value is 3–5, the color difference can be observed by an average consumer (Ghidouche, Rey, Michel, & Galaffu, 2013). An Δ*Eab* value of up to 10 is considered to indicate an acceptable color change for iron-fortified salts (Wegmüller, Zimmermann, & Hurrell, 2003). For all samples the Δ*Eab* value was > 5, indicating that a color difference could be observed (Fig. 3**C**).

For the samples in the presence of the water-soluble phenolics (i.e., epicatechin, caffeic acid, and catechol), an absorbance band was observed with $\lambda_{max} \sim 580$ nm (Fig. 3**A**). This broad absorbance band is due to the ligand-to-metal charge transfer (LMCT) phenomenon. This absorbance band with $\lambda_{max} \sim 580$ nm is typically observed for Fe(III)-catechol complexes with a stoichiometry of 1:2 at pH ranging from 5 to 7 (Bijlsma et al., 2020; Elhabiri, Carrër, Marmolle, & Traboulsi, 2007) and causes the bluish to purplish appearance of the supernatants (Fig. 3**B**). Moreover, in the presence of the water-soluble phenolics, the precipitate changed from white to a greyish/bluish color. We hypothesized previously that the discoloration of the precipitates at pH 6.5 can be due to the formation of Fe(III)-phenolic complexes at the surface of the salts (Moslehi et al., 2022), which is further discussed in section 3.4. In line with these color changes in the supernatant and precipitate, the Δ*Eab* differences for water-soluble phenolics in presence of the Fe(III)-containing salts were unacceptable and much larger than for the slightly water-soluble and insoluble phenolics (quercetin, apigenin, and curcumin) (Fig. 3**C**).

In the case of quercetin, increased absorbance in the visual spectra was observed in the presence of FePP and the mixed salt with $x = 0.35$ (Fig. 3**A**). The absorbance band with $\lambda_{max} \sim 570$ nm is due to the LMCT phenomenon and the increase in the intensity of absorbance at 450 nm is due to the bathochromic shift of the cinnamoyl band of quercetin (Bijlsma et al., 2022). In the absence of any of the iron-containing salts or in the presence of the mixed salts with $x \leq 0.18$, the supernatant of the quercetin sample did not show any absorbance due to the poor solubility of quercetin in water. The increased absorbance observed in the supernatant in presence of the salts with $x = 0.35$ and $x = 1$ is suggested to be a result of the formation of a charged Fe(III)-quercetin complex that improves the solubility of quercetin (Malacaria et al., 2022). For apigenin and curcumin, no increase in absorbance was observed in the presence of iron-containing salts (Fig. 3**A**), in line with the transparent supernatants of these samples (Fig. 3**B**). For the supernatants of quercetin in the presence of CaPP and the mixed salts (with $x \leq 0.18$) and for apigenin and curcumin in presence of all salts the Δ*Eab* value was at maximum around 10. The images of apigenin indicate that the precipitates in the presence of FePP and the mixed salt with $x = 0.35$ turned dark brown. Additionally, for curcumin a slightly darker layer was observed on the precipitate in the presence of FePP (Fig. 3**B**). This indicates that complexation reactions between iron and apigenin or curcumin occurred, but the formed products remained insoluble. This is most likely for one or a combination of the following three reasons: (i) Fe (III)-phenolic complexation at the surface of the undissolved salt particles, (ii) the formation of neutral and/or insoluble complexes of iron with these phenolics (Malacaria et al., 2022), or (iii) the inherently poor solubility of these phenolics (**supplementary information**, **Fig. S4**). In line with the observed discoloration in the precipitate (Fig. 3**B**), the Δ*Eab* value of quercetin and apigenin in the presence of FePP or the salt with $x = 0.35$ was unacceptable (>10). The Δ*Eab* value for the precipitate of curcumin in the presence of the salts with $x \leq 0.15$ was also > 10. This apparent color change to lighter shades of orange (lightness $L^* = 48$ for blank versus $L^* = 64$ for CaPP) is resulting from the presence of white or off-white insoluble pyrophosphate salts in these precipitates that mix with curcumin, compared to the orange color of pure curcumin (blank), rather than from dark-color formation.

We observed that the intensity of the LMCT absorbance band (Fig. 3**A**) increased monotonically with the x-value of the mixed Ca-Fe (III) pyrophosphate salts. For the mixed salts with $0 \leq x \leq 0.35$ in presence of catechol, caffeic acid, epicatechin, and quercetin, the area under the curve in the visible range ($AUC_{380\text{-}750}$) showed a linear relationship with the iron concentration in solution ($R^2 > 0.97$) (**supplementary information**, **Fig. S7**). For epicatechin and quercetin the $R^2$ value decreased from 0.995 to 0.970 and from 0.990 to 0.872,

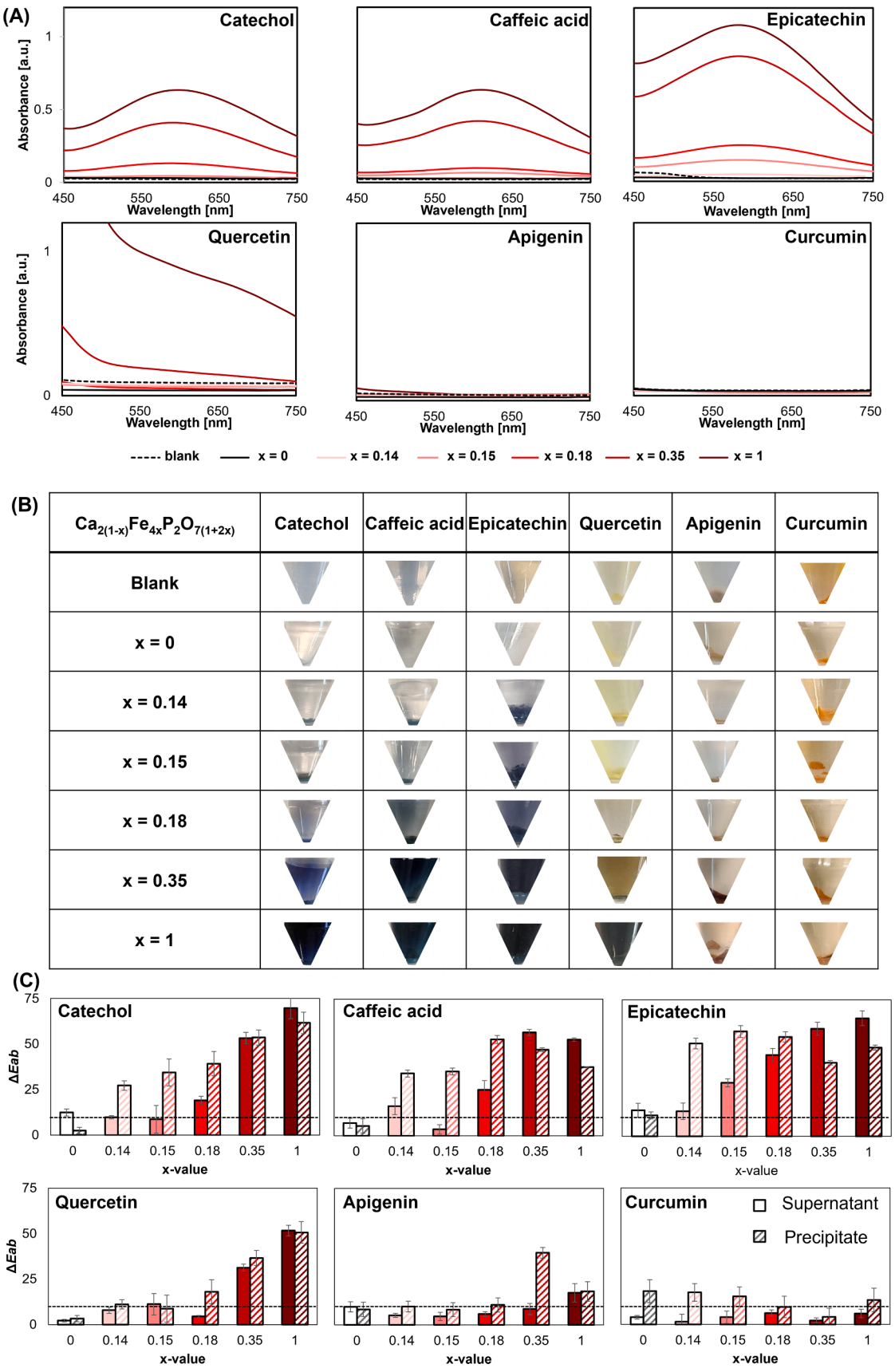


**Fig. 3.** (A) Absorbance spectra of the supernatants of CaPP, FePP, and the mixed Ca-Fe(III) pyrophosphate salts in the presence of the different phenolics at pH 6. The dashed lines indicate the absorbance of the pure phenolics (in the absence of the salts). (B) Pictures of the supernatants and precipitates in the Eppendorf tubes. (C) The values of Δ*Eab* correspond to the color changes in the supernatant (filled bar) and precipitate (striped bar) after being exposed to CaPP, FePP, and the mixed Ca-Fe(III) pyrophosphate salts, compared to no salts (i.e. blank phenolics). The dashed line indicates the maximum acceptable color change (i.e., Δ*Eab* = 10).

respectively, if the point corresponding to FePP (x = 1) was included, because the slope of $AUC_{380\text{-}750}$ suddenly increased from x = 0.35 to x = 1. It has previously been shown that the inclusion of the divalent metals (i.e., M(II)), such as calcium, can change the dark-colored iron-phenolic complexation product towards a colorless M(II)-phenolic reaction product via metal competition for complexation with phenolics (Guo et al., 2014). If this competition would occur in these samples, then we would expect this relation between $AUC_{380\text{-}750}$ and iron concentration to be non-linear, because the samples at lower x-value contain relatively more Ca compared to higher x-values (i.e., for x = 0.14 Ca/Fe = 3.1 and for x = 0.35 the Ca/Fe = 0.93). However, our findings show a direct linear relationship between the iron concentration and color, thus we conclude that the effect of metal competition on color was likely very limited in these samples. We suggest that competition is limited because Fe(III) is a harder Lewis acid compared to Ca, and therefore a much larger excess of Ca (i.e. Ca/Fe ≥ 10) should be present to effectively limit color change via metal competition (Habeych et al., 2016).

Overall, for water-soluble phenolics, the use of mixed Ca-Fe(III) pyrophosphate salts did not protect against adverse color changes that are caused by iron-phenolic complexation, as is indicated by the observed color change and presence of the LMCT band in the absorbance spectra. For quercetin, apigenin, and curcumin, the color change was limited to acceptable values ($\Delta Eab \sim 10$) in the presence of salts with x ≤ 0.18. These outcomes show that the mixed Ca-Fe(III) pyrophosphate salts are more suitable for fortification of food products that do not contain water-soluble phenolic compounds. Moreover, these findings explain why the mixed salts show comparable reactivity to FePP in a model black tea solution, which mainly contains water-soluble phenolics (Moslehi et al., 2022).

### 3.3. Oxidation rate of phenolics in the presence of the CaPP, FePP, and mixed Ca-Fe(III) pyrophosphate salts

Complexation reactions can be succeeded by oxidation reactions of phenolics because the complexation can be followed by an electron transfer from the ligand to Fe(III) (Ryan & Hynes, 2008). Subsequent reactions of the oxidized phenolics yield a plethora of products that can arise from phenolic degradation and oxidative coupling. Because of the extended conjugated system of phenolics after oxidative coupling, these products may also contribute to discoloration (Tan, de Bruijn, van Zadelhoff, Lin, & Vincken, 2020). To date, the effect of FePP and mixed Ca-Fe(III) pyrophosphate salts on phenolic oxidation is unknown. Therefore, we quantified the recovery of phenolics after incubation in the presence of the studied pyrophosphate salts at selected pH values (i.e., 3, 6, and 8) by RP-UHPLC-PDA-$MS^n$ (Fig. 4). Epicatechin and quercetin were chosen as representatives for water-soluble and slightly soluble/insoluble categories of the studied phenolics, respectively.

At pH 3, no significant difference ($p > 0.05$) was observed in the recovery of epicatechin in the presence of the different pyrophosphate salts (Fig. 4**A**). Because the hydroxyl groups are protonated at pH 3 (Fig. 1), no complexation or subsequent oxidation reactions occurred at pH 3. In the case of quercetin at pH 3, a significant decrease in recovery was observed for the blank and in presence of the different salts. (Fig. 4**B**). These differences could not be linked to the x-value of the salts, and because no oxidation products were detected in these samples (results not shown) it remains unclear why significantly different recoveries were observed at pH 3. Possibly some quercetin was lost due to the poor solubility and adsorption on the electrode during pH adjustment. At pH 6, a significant decrease ($p < 0.05$) in the recovery of epicatechin and quercetin in the presence of FePP (x = 1) was observed compared to the blank, CaPP, and all mixed Ca-Fe(III) pyrophosphate salts. The significant decrease in intact epicatechin and quercetin by 35% and 55% of their initial amount, respectively, after 2 h of exposure to the FePP is suggested to be due to oxidation of the phenolic compounds. This was supported by an increase in peak areas of the main oxidation products from epicatechin (δ-type dehydrocatechin) and quercetin (2,4,6-trihydroxyphenyl glyoxylic acid and 3,4-dihydroxybenzoic acid) upon increasing x-value (**supplementary information**, **Fig. S8**, and **Fig. S9**) (Bijlsma et al., 2022; Tan et al., 2020). For quercetin, more oxidative degradation products rather than oxidative coupling products were observed compared to epicatechin due to the presence of the 3-OH group in conjugation with the *C2-C3* double bond, which enables formation of the highly reactive quinone methides as intermediates in the degradation of quercetin (Stepanic, Gasparovic, Troselj, Amic, & Zarkovic, 2015).

Faster oxidation of the phenolics in the presence of FePP at pH 6 can be linked to a higher degree of complexation as shown in section 3.2. Exposure to FePP resulted in the most intense discoloration caused by more complex formation of quercetin and epicatechin with iron ions. After 2 h incubation of epicatechin at pH 8 in the presence of FePP, the epicatechin concentration significantly decreased compared to incubation of the blank or in the presence of CaPP ($p < 0.05$) (Fig. 4**A**). The concentration of recovered epicatechin was not significantly different in the presence of the various mixed Ca-Fe(III) pyrophosphate salts. Similarly, no significant difference between the salts could be found for quercetin because its fast oxidation in the presence of the Fe(III)-containing pyrophosphate salts at pH 8 resulted in concentrations being below the limit of quantification. However, in the blank or in presence of CaPP, a significantly higher amount of quercetin was recovered compared to all iron-containing salts.

At food-relevant pH (i.e., 6), the inclusion of calcium in the Fe(III)-containing pyrophosphate salts resulted in less oxidation of the phenolic compound compared to pure FePP. This is the first indication that fortification of foods with mixed Ca-Fe(III) pyrophosphate salts

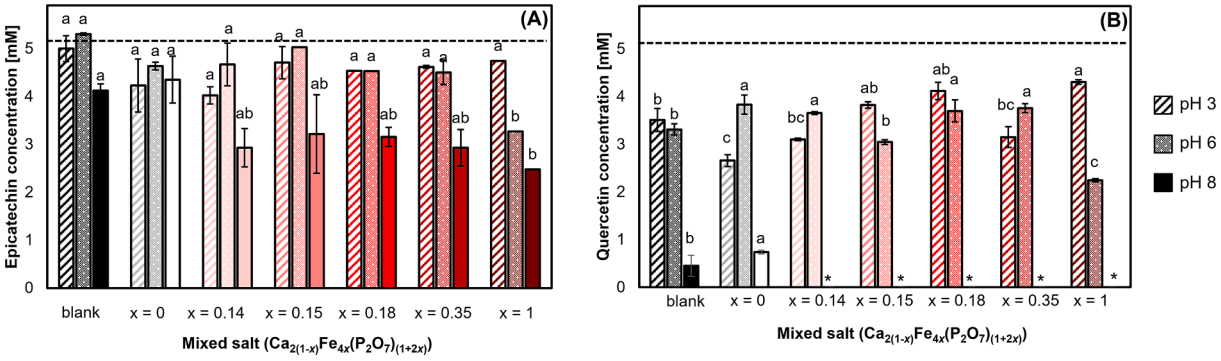


**Fig. 4.** Recovery of (A) epicatechin and (B) quercetin in the absence and presence of the different salts at pH 3 (striped bar), 6 (dotted bar), and 8 (filled bar) after incubation for 2 h at 23 °C. The error bars indicate the standard deviation of independent duplicates. The dashed line indicates the initial concentration of the phenolics (5 mM). Different letters indicate a significant difference in the concentration compared to the other x-values for the same pH value (Tukey's test, $p < 0.05$). * indicates that the concentration was below the limit of quantification.

instead of pure FePP can potentially limit the extent of iron-mediated food oxidation. Even though oxidation is already limited to a certain extent in the presence of FePP compared to $FeSO_4$, because of the decreased soluble iron concentration (Wegmüller et al., 2003; Zuidam, 2012), inclusion of calcium in the Ca-Fe(III) pyrophosphate salts further lowers the soluble iron concentration, thereby further limiting phenolic oxidation as well. Another added benefit of the limited phenolic oxidation in the presence of the mixed Ca-Fe(III) pyrophosphate salts is inhibition of the formation of the potentially toxic or mutagenic oxidative degradation products of quercetin upon iron-fortification (Harwood, Danielewska-Nikiel, Borzelleca, Flamm, Williams, & Lines, 2007). Besides oxidation of phenolics, oxidation of fatty acids, amino acids, and other micronutrients may also occur in presence of Fe(III) (Zuidam, 2012). It should be further investigated whether these iron-mediated oxidation reactions are also limited in the presence of the mixed Ca-Fe(III) pyrophosphate, compared to FePP.

### 3.4. Surface composition of CaPP, FePP, and mixed Ca-Fe(III) pyrophosphate salts in the absence and presence of phenolics

The mixed Ca-Fe(III) pyrophosphate salts based on the general formula, $Ca_{2(1-x)}Fe_{4x}(P_2O_7)_{(1+2x)}$ with a theoretical x-value $< 0.33$ contain a lower percentage of Fe compared to Ca in bulk. This Ca/Fe $> 1$ has previously been confirmed for the salts with $x \leq 0.18$ by TEM-EDX (Moslehi et al., 2022), and is indicated by the ratios of Fe/P and Ca/P for the salts as shown in Fig. 5**A**. We hypothesized that the incorporation of calcium as a second mineral along with iron in the pyrophosphate matrix would reduce the iron content at the surface of the mixed Ca-Fe (III) pyrophosphate salts and thereby lower the soluble iron concentration and iron-mediated reactivity. XPS measurements were employed to find the elemental composition at the surface of these salts (Fig. 5**B**, wide scan XPS spectra in the **supplementary information**, **Fig. S10**). To interpret the data, the elemental percentages of the salts obtained from XPS were normalized with respect to phosphorus. It was confirmed that FePP and all the mixed salts contained a lower iron to phosphorus ratio (Fe/P) at the surface than in the bulk, with up to a 5.5-fold decrease in the case of the mixed salt with $x = 0.14$. This variation in distribution of iron elements in the salt matrix (i.e., surface vs bulk) can be caused by the higher dissolution of Fe ions than Ca ions from the surface of the pyrophosphate salts in water at the pH of the reaction mixture which results in higher Fe solubilization from the salts during the washing steps for purification (Moslehi et al., 2022; van Leeuwen, 2013). This solubilization of Fe from the surface of the salts can be experimentally linked to the negative surface charge of the salts particles in their colloidal state (before drying to powder) at this pH range as well (data not shown here). However, comparing the calcium to phosphorus ratio (Ca/P) in the bulk and at the surface of the salts showed that this ratio was the same or slightly lower (on average 1.18 ± 0.18-fold). These results suggest that the mixed pyrophosphate salts have a lower iron to calcium ratio at their surface compared to their bulk composition, despite having homogeneous elemental distribution throughout their aggregates (Moslehi et al., 2022).

The XPS measurements were also utilized to obtain the carbon to phosphorus ratio (C/P) as an indication of the presence of phenolics on the surface of the salts. Accurate determination of elemental ratios of carbon in the bulk using TEM-EDX was not possible due to the carbon film on the TEM grids. The XPS measurements indicated that after exposing the salts to epicatechin and removal of the free epicatechin by washing with water, C/P at the surface of the salts increased noticeably, by up to 13-fold (Fig. 5**C**, wide scan XPS spectra in the **supplementary information**, **Fig. S11**). Although the minor amounts of carbon present in XPS spectra are inevitable (e.g., due to the presence of atmospheric carbon dioxide impurities), this considerable increase in the carbon content at the surface of the Fe(III)-containing iron salts is additional confirmation, besides the color of the precipitates, for the presence of epicatechin at the surface of the insoluble pyrophosphate salts. In addition, Fe/P at the surface of the iron-containing salts decreased substantially, up to a 3.2-fold, after incubation with epicatechin, whereas the Ca/P ratio remained similar (Fig. 5**C**). This indicates that besides binding of Fe at the surface of the salt by epicatechin, a significant proportion of Fe was released into the solution after complexation with epicatechin, which is in line with the increased soluble iron concentration in the presence of epicatechin (Fig. 2, and **supplementary information**, **Fig. S12**). Furthermore, it is possible that a fraction of Fe at the surface of these salts is covered by the bound epicatechin and therefore the detection intensity of iron can be decreased in XPS measurements due to this spatial hindrance.

### 3.5. Possible mechanism for reactivity of iron from FePP and mixed Ca-Fe (III) pyrophosphate salts

This study demonstrated that the dissolution behavior of iron from FePP and mixed Ca-Fe(III) pyrophosphate salts depends on the x-value of the salt, the pH, the solubility of the phenolic compound, and the Fe (III)-coordinating group(s) of the phenolic compound. Fig. 6 schematically summarizes the fate of the Fe(III)-containing pyrophosphate salts with different x-values in the absence and presence of phenolics at pH 6–6.5 (representative for food products).

In the absence of phenolics, the salts with $x \leq 0.18$ show up to an eightfold decrease in soluble iron concentration compared to FePP. In the presence of water-soluble phenolics, the color of both the supernatant and the precipitate is negatively affected. Firstly, the precipitate turns dark due to interactions of the water-soluble phenolic with iron present at the surface of the salts. Secondly, after binding the water-soluble phenolic to the iron at the surface, the iron-phenolic complex releases into solution and becomes soluble, causing discoloration of the

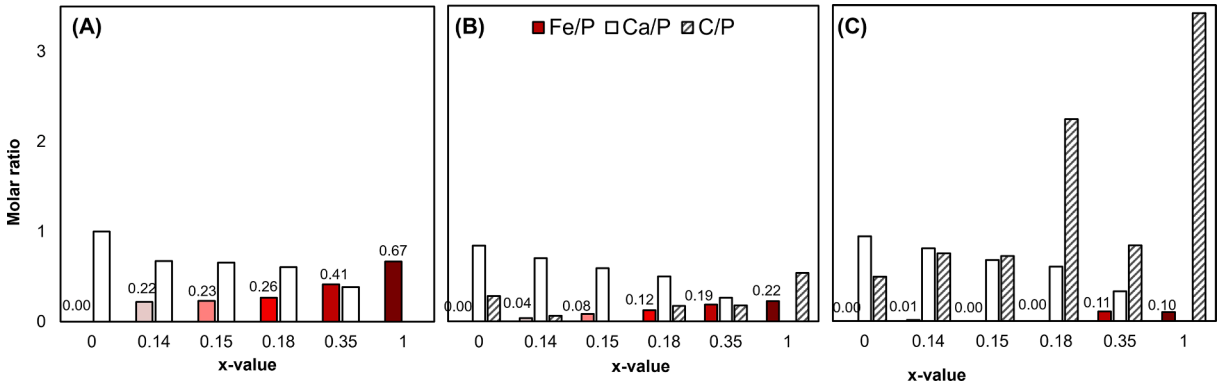


**Fig. 5.** Analysis of the elemental composition of the CaPP, FePP, and mixed Ca-Fe(III) pyrophosphate salts (A) in the bulk by TEM-EDX obtained from (Moslehi et al., 2022), (B) at the surface by XPS, and (C) at the surface after reactivity with epicatechin at pH 6. The data labels on the bars indicate the Fe/P ratios.

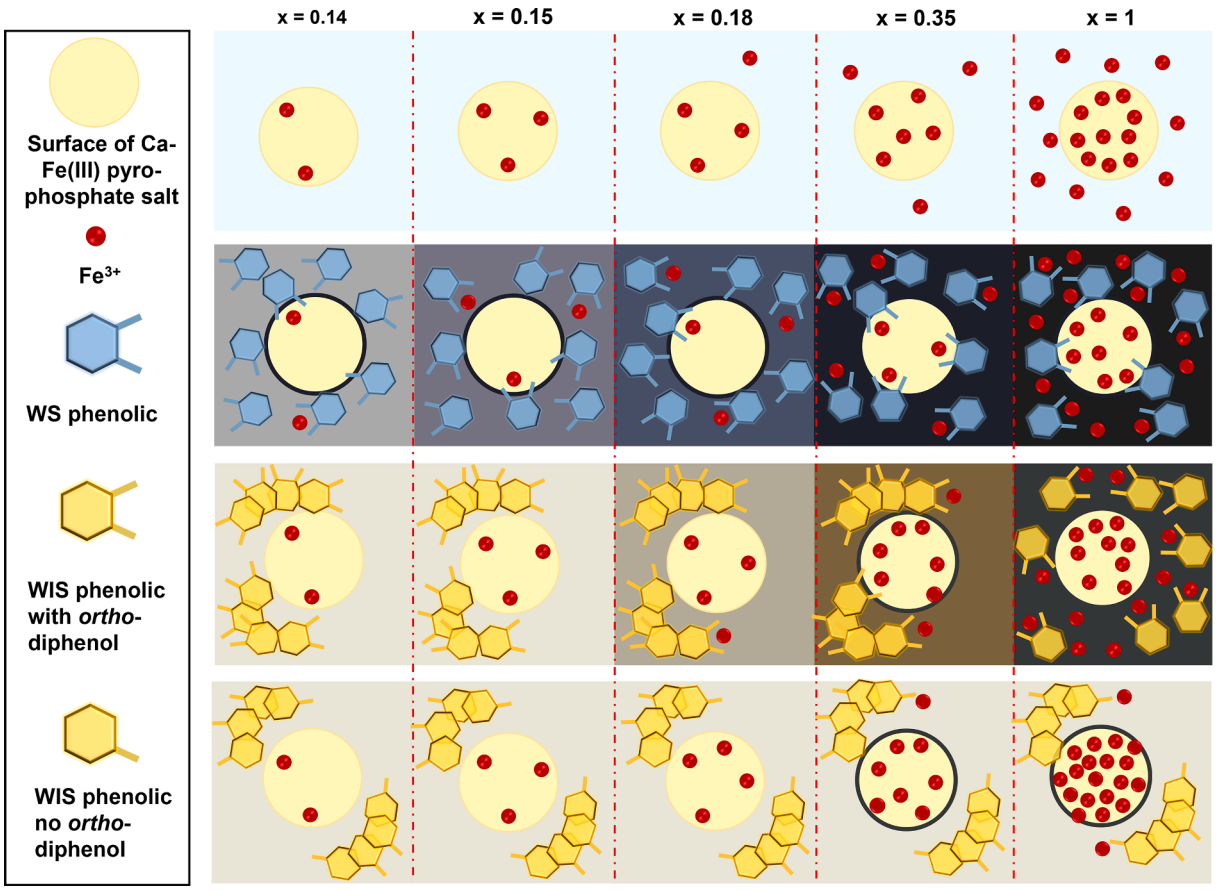


**Fig. 6.** Schematic overview of the proposed mechanism underlying the observed dissolution behavior of iron at the surface of the FePP (x = 1) and mixed Ca-Fe(III) pyrophosphate salts with x = 0.14, 0.15, 0.18, and 0.35, and the reactivity of iron from these salts in the presence of phenolics at pH 6. The colors in the squares are in line with the experimentally observed color of the supernatant, a dark outline on the salt surface indicates the discoloration observed in the precipitate. WS = water-soluble, WIS = slightly water-soluble or water-insoluble.

supernatant. For slightly water-soluble and insoluble phenolics with an *ortho*-diphenolic group, we suggest that the soluble iron can form stable charged complexes that are solubilized in water, leading to discoloration in both the supernatant and precipitate. For slightly water-soluble and insoluble phenolics without the *ortho*-diphenolic group, there is no interaction between the iron and the phenolic for the mixed salts with x $\leq$ 0.18. If iron is already present in the solution (i.e., x = 0.35 and 1), it can coordinate with the insoluble phenolic and cause discoloration in the precipitate but these Fe(III)-phenolic coordinates remain insoluble. The schematic overview in Fig. 6 only applies when the pH is above the apparent $pK_a$ of the phenolic compounds, as deprotonation of the phenolic hydroxyl groups is a prerequisite for these interactions.

This is the first study to report that the reactivity of Fe(III)-containing pyrophosphate salts in the presence of phenolic compounds is dependent on the solubility and iron-coordinating groups of the phenolic. Understanding the reactivity of the mixed pyrophosphate salts with phenolics is helpful for the application of these salts in the design of iron-fortified food products. The present findings show that these salts are potential iron-fortificants for application in food products that mainly contain poorly water-soluble phenolic compounds, such as savory concentrates. In future studies, the reactivity of the mixed salts can be assessed in real food products and in the presence of product-specific mixtures of phenolic compounds.

## 4. Conclusions

In this study, we investigated the reactivity of FePP and mixed Ca-Fe (III) pyrophosphate salts (based on the general formula $Ca_{2(1-x)}Fe_{4x}(P_2O_7)_{(1+2x)}$ with $0 \leq x \leq 1$) in the presence of six different phenolic compounds. Besides iron-phenolic reactivity, which results in complexation and oxidation, the effect of the presence of phenolic compounds on iron solubility from the salts was also assessed. At pH 5–7, the water-soluble phenolics (i.e., catechol, caffeic acid, and epicatechin) increased iron solubility from the mixed pyrophosphate salts by up to 11-fold, by solubilization of iron from the surface of the salts. This led to unacceptable discoloration as a result of Fe(III)-phenolic complexation. In the presence of the slightly water-soluble (i.e., quercetin and apigenin) and insoluble phenolics (i.e., curcumin), iron from the salts remained practically insoluble. Furthermore, for the salts with x $\leq$ 0.18, the color change after exposure to these poorly water-soluble phenolics remained acceptable for application. In addition, all mixed Ca-Fe(III) pyrophosphate salts resulted in significantly less oxidation of epicatechin and quercetin at pH 6 compared to FePP. In conclusion, mixed pyrophosphate salts with x $\leq$ 0.18 cause limited iron-mediated discoloration and oxidation. Thereby, they can potentially be used in designing iron-fortified foods containing slightly water-soluble and/or water-insoluble phenolics. In future studies, the reactivity of these salts in real food products, along with associated changes in other organoleptic properties should be investigated. Additionally, the *in vivo* iron bioavailability and the potential of these salts as dual-fortificants have to be investigated in future work.

## Funding Source

This research received funding from the Netherlands Organization for Scientific Research (NWO) in the framework of the Innovation Fund

for Chemistry and from the Ministry of Economic Affairs in the framework of the "*TKI/PPS-Toeslagregeling*" (Grant 731017205).

## CRediT authorship contribution statement

**Judith Bijlsma:** Conceptualization, Methodology, Investigation, Visualization, Writing – original draft. **Neshat Moslehi:** Conceptualization, Methodology, Investigation, Visualization, Writing – original draft. **Krassimir P. Velikov:** Conceptualization, Methodology, Supervision, Writing – review & editing. **Willem K. Kegel:** Conceptualization, Supervision, Writing – review & editing. **Jean-Paul Vincken:** Conceptualization, Supervision, Writing – review & editing. **Wouter J.C. De Bruijn:** Conceptualization, Methodology, Supervision, Writing – review & editing.

## Declaration of Competing Interest

The authors declare that they have no known competing financial interests or personal relationships that could have appeared to influence the work reported in this paper.

## Data availability

Data will be made available on request.

## Acknowledgements

The authors are grateful to Barend van Lagen (Organic Chemistry, Wageningen University & Research) for performing the XPS measurements. Arjen Reichwein, Raymond Nijveld, and Teun de Bruin of Nouryon Chemicals B.V. are thanked for performing the ICP-AES measurements. The graphical abstract was made with content from BioRender.com.

## Appendix A. Supplementary data

Supplementary data to this article can be found online at https://doi.org/10.1016/j.foodchem.2022.135156.

## References

Allen, L. H., De Benoist, B., Dary, O., & Hurrell, R. (Eds.). (2006). *Guidelines on food fortification with micronutrients*. Geneva, Switzerland: World Health Organization.

Andre, C. M., Evers, D., Ziebel, J., Guignard, C., Hausman, J.-F., Bonierbale, M., … Burgos, G. (2015). In vitro bioaccessibility and bioavailability of iron from potatoes with varying vitamin C, carotenoid, and phenolic concentrations. *Journal of Agricultural and Food Chemistry, 63*(41), 9012–9021. https://doi.org/10.1021/acs.jafc.5b02904

Araki, H., Kim, J., Zhang, S., Banks, A., Crawford, K. E., Sheng, X., … Rogers, J. A. (2017). Materials and device designs for an epidermal UV colorimetric dosimeter with near field communication capabilities. *Advanced Functional Materials, 27*(2), 1604465. https://doi.org/10.1002/adfm.201604465

Bijlsma, J., de Bruijn, W. J. C., Hageman, J. A., Goos, P., Velikov, K. P., & Vincken, J.-P. (2020). Revealing the main factors and two-way interactions contributing to food discolouration caused by iron-catechol complexation. *Scientific Reports, 10*(1), 1–11. https://doi.org/10.1038/s41598-020-65171-1

Bijlsma, J., de Bruijn, W. J. C., Velikov, K. P., & Vincken, J.-P. (2022). Unravelling discolouration caused by iron-flavonoid interactions: Complexation, oxidation, and formation of networks. *Food Chemistry, 370*, Article 131292. https://doi.org/10.1016/j.foodchem.2021.131292

Delgado, A. M., Issaoui, M., & Chammem, N. (2019). Analysis of main and healthy phenolic compounds in foods. *Journal of AOAC International, 102*(5), 1356–1364. https://doi.org/10.1093/jaoac/102.5.1356

Dueik, V., Chen, B. K., & Diosady, L. L. (2017). Iron-polyphenol interaction reduces iron bioavailability in fortified tea: Competing complexation to ensure iron bioavailability. *Journal of Food Quality, 2017*, 7. https://doi.org/10.1155/2017/1805047

El-Sherif, A. A., Shoukry, M. M., & Abd-Elgawad, M. M. A. (2013). Protonation equilibria of some selected α-amino acids in DMSO–water mixture and their Cu(II)-complexes. *Journal of Solution Chemistry, 42*(2), 412–427. https://doi.org/10.1007/s10953-013-9966-0

Elhabiri, M., Carrër, C., Marmolle, F., & Traboulsi, H. (2007). Complexation of iron(III) by catecholate-type polyphenols. *Inorganica Chimica Acta, 360*(1), 353–359. https://doi.org/10.1016/j.ica.2006.07.110

Ghidouche, S., Rey, B., Michel, M., & Galaffu, N. (2013). A rapid tool for the stability assessment of natural food colours. *Food Chemistry, 139*(1), 978–985. https://doi.org/10.1016/j.foodchem.2012.12.064

Giesbers, M., Marcelis, A. T. M., & Zuilhof, H. (2013). Simulation of XPS C1s spectra of organic monolayers by quantum chemical methods. *Langmuir, 29*(15), 4782–4788. https://doi.org/10.1021/la400445s

Guo, J., Ping, Y., Ejima, H., Alt, K., Meissner, M., Richardson, J. J., … Hagemeyer, C. E. (2014). Engineering multifunctional capsules through the assembly of metal–phenolic networks. *Angewandte Chemie International Edition, 53*(22), 5546–5551. https://doi.org/10.1002/anie.201311136

Habeych, E., van Kogelenberg, V., Sagalowicz, L., Michel, M., & Galaffu, N. (2016). Strategies to limit colour changes when fortifying food products with iron. *Food Research International, 88*, 122–128. https://doi.org/10.1016/j.foodres.2016.05.017

Harwood, M., Danielewska-Nikiel, B., Borzelleca, J. F., Flamm, G. W., Williams, G. M., & Lines, T. C. (2007). A critical review of the data related to the safety of quercetin and lack of evidence of in vivo toxicity, including lack of genotoxic/carcinogenic properties. *Food and Chemical Toxicology, 45*(11), 2179–2205. https://doi.org/10.1016/j.fct.2007.05.015

Hider, R. C., Liu, Z. D., & Khodr, H. H. (2001). Metal chelation of polyphenols. In *Methods in enzymology* (pp. 190–203). Elsevier.

Hurrell, R. (2002). How to ensure adequate iron absorption from iron-fortified food. *Nutrition Reviews, 60*, S7–S15. https://doi.org/10.1301/002966402320285137

Hurrell, R. F., Lynch, S., Bothwell, T., Cori, H., Glahn, R., Hertrampf, E., … Zimmermann, M. B. (2004). Enhancing the absorption of fortification iron. *International Journal for Vitamin and Nutrition Research, 74*(6), 387–401. https://doi.org/10.1024/0300-9831.74.6.387

Janssen, R. H., Canelli, G., Sanders, M. G., Bakx, E. J., Lakemond, C. M., Fogliano, V., & Vincken, J.-P. (2019). Iron-polyphenol complexes cause blackening upon grinding *Hermetia illucens* (black soldier fly) larvae. *Scientific Reports, 9*(1), 2967. https://doi.org/10.1038/s41598-019-38923-x

Kasprzak, M. M., Erxleben, A., & Ochocki, J. (2015). Properties and applications of flavonoid metal complexes. *RSC Advances, 5*(57), 45853–45877. https://doi.org/10.1039/C5RA05069C

Liangou, A., Florou, K., Psichoudaki, M., Kostenidou, E., Tsiligiannis, E., & Pandis, S. N. (2022). A method for the measurement of the water solubility distribution of atmospheric organic aerosols. *Environmental Science & Technology, 56*(7), 3952–3959. https://doi.org/10.1021/acs.est.1c06854

Malacaria, L., Corrente, G. A., Beneduci, A., Furia, E., Marino, T., & Mazzone, G. (2021). A review on coordination properties of Al(III) and Fe(III) toward natural antioxidant molecules: Experimental and theoretical insights. *Molecules, 26*(9), 2603. https://doi.org/10.3390/molecules26092603

Malacaria, L., La Torre, C., Furia, E., Fazio, A., Caroleo, M. C., Cione, E., … Plastina, P. (2022). Aluminum(III), iron(III) and copper(II) complexes of luteolin: Stability, antioxidant, and anti-inflammatory properties. *Journal of Molecular Liquids, 345*, Article 117895. https://doi.org/10.1016/j.molliq.2021.117895

Mohammed, F., Rashid-Doubell, F., Cassidy, S., & Henari, F. (2017). A comparative study of the spectral, fluorometric properties and photostability of natural curcumin, iron- and boron-complexed curcumin. *Spectrochimica Acta Part A: Molecular and Biomolecular Spectroscopy, 183*, 439–450. https://doi.org/10.1016/j.saa.2017.04.027

Moretti, D., Hurrell, R. F., & Cercamondi, C. I. (2018). Bouillon cubes. In *Food fortification in a globalized world* (pp. 159–165). Elsevier.

Moslehi, N., Bijlsma, J., De Bruijn, W. J. C., Velikov, K. P., Vincken, J.-P., & Kegel, W. K. (2022). Design and characterization of Ca-Fe(III) pyrophosphate salts with tunable pH-dependent solubility for dual-fortification of foods. *Journal of Functional Foods, 92*, Article 105066. https://doi.org/10.1016/j.jff.2022.105066

Nkhili, E., Loonis, M., Mihai, S., El Hajji, H., & Dangles, O. (2014). Reactivity of food phenols with iron and copper ions: Binding, dioxygen activation and oxidation mechanisms. *Food & Function, 5*(6), 1186–1202. https://doi.org/10.1039/C4FO00007B

Perron, N. R., & Brumaghim, J. L. (2009). A review of the antioxidant mechanisms of polyphenol compounds related to iron binding. *Cell Biochemistry and Biophysics, 53*(2), 75–100. https://doi.org/10.1007/s12013-009-9043-x

Poynton, C. (2012). *Digital video and hd: Algorithms and interfaces*. Waltham, MA, USA: Elsevier.

Ryan, P., & Hynes, M. J. (2008). The kinetics and mechanisms of the reactions of iron(III) with quercetin and morin. *Journal of Inorganic Biochemistry, 102*(1), 127–136. https://doi.org/10.1016/j.jinorgbio.2007.07.041

Silva, A., Kong, X., & Hider, R. C. (2009). Determination of the pKa value of the hydroxyl group in the α-hydroxycarboxylates citrate, malate and lactate by 13C NMR: Implications for metal coordination in biological systems. *Biometals, 22*(5), 771–778. https://doi.org/10.1007/s10534-009-9224-5

Sorkun, M. C., Khetan, A., & Er, S. (2019). AqSolDB, a curated reference set of aqueous solubility and 2D descriptors for a diverse set of compounds. *Scientific Data, 6*(1), 143. https://doi.org/10.1038/s41597-019-0151-1

Stepanic, V., Gasparovic, A. C., Troselj, K. G., Amic, D., & Zarkovic, N. (2015). Selected attributes of polyphenols in targeting oxidative stress in cancer. *Current Topics in Medicinal Chemistry, 15*(5), 496–509. https://doi.org/10.2174/1568026615666150209123100

Stookey, L. L. (1970). Ferrozine: A new spectrophotometric reagent for iron. *Analytical Chemistry, 42*(7), 779–781. https://doi.org/10.1021/ac60289a016

Swain, J. H., Newman, S. M., & Hunt, J. R. (2003). Bioavailability of elemental iron powders to rats is less than bakery-grade ferrous sulfate and predicted by iron

solubility and particle surface area. *The Journal of Nutrition, 133*(11), 3546–3552. https://doi.org/10.1093/jn/133.11.3546

Tan, J., de Bruijn, W. J. C., van Zadelhoff, A., Lin, Z., & Vincken, J.-P. (2020). Browning of epicatechin (EC) and epigallocatechin (EGC) by auto-oxidation. *Journal of Agricultural and Food Chemistry, 68*(47), 13879–13887. https://doi.org/10.1021/acs.jafc.0c05716

Tian, T., Blanco, E., Smoukov, S. K., Velev, O. D., & Velikov, K. P. (2016). Dissolution behaviour of ferric pyrophosphate and its mixtures with soluble pyrophosphates: Potential strategy for increasing iron bioavailability. *Food Chemistry, 208*, 97–102. https://doi.org/10.1016/j.foodchem.2016.03.078

van Leeuwen, Y. M. (2013). *Colloidal metal pyrophosphate salts: Preparation, properties and applications*. Utrecht: Utrecht University. Ph.D. Thesis.

Wegmüller, R., Zimmermann, M. B., & Hurrell, R. F. (2003). Dual fortification of salt with iodine and encapsulated iron compounds: Stability and acceptability testing in Morocco and Côte d'Ivoire. *Journal of Food Science, 68*(6), 2129–2135. https://doi.org/10.1111/j.1365-2621.2003.tb07031.x

Zuidam, N. J. (2012). An industry perspective on the advantages and disadvantages of iron micronutrient delivery systems. In N. Garti, & D. J. McClements (Eds.), *Encapsulation technologies and delivery systems for food ingredients and nutraceuticals* (pp. 505–540). Woodhead Publishing.